Chemical Science

ROYAL SOCIETY OF CHEMISTRY

EDGE ARTICLE

View Article Online
View Journal | View Issue

Cite this: *Chem. Sci.*, 2022, **13**, 8341

All publication charges for this article have been paid for by the Royal Society of Chemistry

Received 18th May 2022
Accepted 22nd June 2022

DOI: 10.1039/d2sc02791g

rsc.li/chemical-science

Enzyme-photo-coupled catalysis in gas-sprayed microdroplets†

Yunxiu Bai,[a] Pengqian Luan,[b] Yunpeng Bai,[c] Richard N. Zare *[d] and Jun Ge *[abe]

Enzyme-photo-coupled catalysis produces fine chemicals by combining the high selectivity of an enzyme with the green energy input of sunlight. Operating a large-scale system, however, remains challenging because of the significant loss of enzyme activity caused by continuous illumination and the difficulty in utilizing solar energy with high efficiency at large scale. We present a large-scale enzyme-photo-coupled catalysis system based on gas-sprayed microdroplets. By this means, we demonstrate a 43.6–71.5 times improvement of solar energy utilization over that using a traditional bulk processing system. Owing to the improved enzyme activity in microdroplets, we show that chiral alcohols can be produced with up to a 2.2-fold increase in the reaction rate and a 5.6-fold increase in final product concentration.

Introduction

Photosynthesis is the largest solar energy utilization system on earth.[1] Such a natural pathway provides a blueprint for scientists to construct an artificial enzyme-photo-coupled (EPC) system to convert solar energy into chemical energy. Since the first artificial photosynthesis system utilizing semiconductors was constructed in 1972 by Fujishima and Honda,[2] EPC catalysis has been widely used for converting solar energy into fuels (such as hydrogen and methanol),[3–6] achieving carbon neutralization,[7–9] and manufacturing high value-added chemicals (such as chiral drug intermediates) in vials.[10–14] Furthermore, EPC is a powerful tool for exploring the catalytic promiscuity of enzymes.[15–19] Great efforts have been made to design catalytic components, as well as to solve the problem of connectivity and compatibility between photocatalysis and enzymatic catalysis, which significantly accelerate the development of EPC catalysis. For example, the use of novel and functional photosensitizers[11,20–22] and enzymes with high activity and broad substrate spectrum engineered by directed evolution[23] has undoubtedly improved catalytic performance. Furthermore, the rational design of the distribution of catalytic components and electron transfer chain inspired by thylakoid in nature improved the overall efficiency of EPC catalysis.[11,24,25] However, most current EPC catalysis studies are conducted at lab scale because of the significant photon transport attenuation effect according to the Lambert–Beer law, which hinders process scale-up.[26–29]

Microdroplets hold promise to address this challenge. Photon transport attenuation can be reduced by converting the bulk solution into microdroplets, thereby significantly reducing the optical path of transmitted light and achieving an increased light intensity. Furthermore, it has been widely reported that reactions can be significantly accelerated in microdroplets[30–38] because of their different concentration distribution, among other reasons. Larger specific surface area and confinement of reagents in microdroplets can significantly increase the reaction rate,[39] whereas some components in microdroplets tend to distribute on the microdroplet surface.[40] An additional favorable feature is that the water microdroplet can act as a spherical lens, focusing incoming parallel radiation from the sun on the back side of the droplet.[41,42] Calculations suggest that this increases the pathlength through the droplet by about 25% compared to the same volume of water in the form of a cube.[43] With these extraordinary properties, microdroplets are expected to be a promising candidate for highly efficient EPC catalysis.

In this study, we described a large-scale EPC catalysis process in microdroplets generated by a continuous gas-spray reactor based on atomization process[44,45] (Fig. 1), which significantly enhanced the light illumination efficiency and resulted in a high overall catalytic rate. More importantly, such a system containing *Sporobolomyces salmonicolor* carbonyl reductase (*Ss*CR), graphite carbon-nitride (GCN), $[Cp^*Rh(bpy)(H_2O)]^{2+}$ (denoted as **M**), cofactor, and triethanolamine (TEOA)

[a]*Key Lab for Industrial Biocatalysis, Ministry of Education, Department of Chemical Engineering, Tsinghua University, Beijing 100084, P. R. China. E-mail: junge@mail.tsinghua.edu.cn*

[b]*Institute of Biomedical Health Technology and Engineering, Shenzhen Bay Laboratory, Shenzhen 518107, P. R. China*

[c]*State Key Laboratory of Bioreactor Engineering, Shanghai Collaborative Innovation Center for Biomanufacturing, East China University of Science and Technology (ECUST), Shanghai 200237, P. R. China*

[d]*Department of Chemistry, Stanford University, Stanford, California 94305-5080, USA. E-mail: zare@stanford.edu*

[e]*Institute of Biopharmaceutical and Health Engineering, Tsinghua Shenzhen International Graduate School, Shenzhen 518055, P. R. China*

† Electronic supplementary information (ESI) available. See https://doi.org/10.1039/d2sc02791g

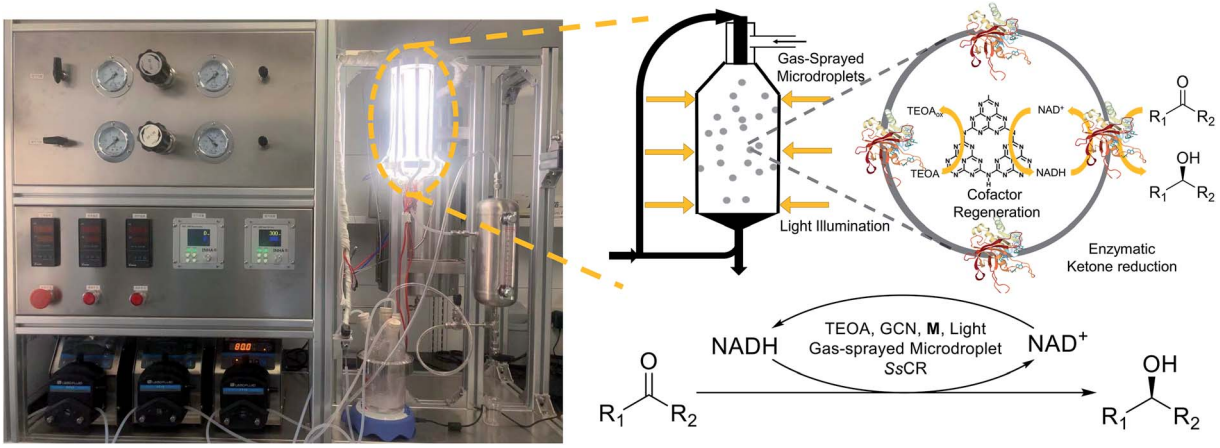

Fig. 1 Picture of gas-spray microdroplet reactor and scheme of enzyme-photo-coupled catalysis system in microdroplets with reagent confinement. NAD, nicotinamide adenine dinucleotide; TEOA, triethanolamine; GCN, graphite-C_3N_4; **M**, $[Cp^*Rh(bpy)(H_2O)]^{2+}$; *Ss*CR, *Sporobolomyces salmonicolor* carbonyl reductase.

generated a significantly higher yield of products. The compartmentalization of the above substances in microdroplets avoided enzyme deactivation and maintained >50% activity after 5 h of illumination compared with rapid and almost complete inactivation of enzyme within 1 h in bulk solution. Therefore, the EPC catalysis in microdroplets showed a 2.2-fold enhancement in initial reaction rate and up to 5.6-fold increase in final product concentration when synthesizing various chiral alcohols. We suggest that this strategy can be a promising platform for highly efficient EPC catalytic processes to solve the limitations in large-scale operations.

Results and discussion

A typical EPC catalysis system is composed of a photosensitizer, an electron transfer intermediate, and a redox enzyme. We used GCN,[46–48] **M**,[49,50] and *Ss*CR[51,52] to construct an EPC catalysis system. TEOA was used as sacrificial electron donor, while GCN was used to absorb light energy, and the excited electrons subsequently reduced NAD^+ into NADH with the assistance of **M**. NADH was eventually utilized for stereoselective reduction of ketones to chiral alcohols, catalyzed by *Ss*CR. Characterizations confirmed the successful synthesis of GCN and its light response characteristics (Fig. S1–S6 in ESI†). The photocatalytic cofactor (reduced nicotinamide adenine dinucleotide, NADH) regeneration and EPC alcohol chiral reduction reaction was first performed in the bulk solution, confirming the successful construction of the reaction system (Fig. S7 and S8 in ESI†).

In the gas-spray microdroplet reactor shown in Fig. 1, a high-velocity inert gas atomized a bulk solution through a two-fluid nozzle located on the top of the reactor. The light source was mounted on the outside of the reactor and uniformly illuminated the microdroplets. The fluid containing the microdroplets was then collected and passed through a gas–liquid separator to recover the inert gas from the reaction solution. In order to avoid evaporation of microdroplets during subsequent catalysis process, the inert gas was partial recycled, thus enhancing the humidity. It is also feasible to pre-humidify the inert gas. The reaction solution was collected and sent back into the feedstock storage tank, where it again underwent the abovementioned process. The flow rates of gas and liquid phases were kept constant to manipulate droplet properties and reaction time. The temperature of the reaction solution and inert gas was also maintained constant using heating insulation equipment. The detailed reactor design and scheme are shown in ESI and Fig. S9.†

The size of microdroplets was studied at different gas velocities using a high-speed charge-coupled device camera (Fig. S10 in ESI†). The results showed that as gas velocity increased, microdroplet diameter gradually decreased (Fig. 2a). Although the decrease in microdroplet size caused by the increase in gas velocity can increase the specific surface area of microdroplets, the high gas velocity in the reactor can result in a large pressure difference, which is undesirable for system pressure resistance and stability. Meanwhile, after the gas rate reached 15 L min^{-1}, the microdroplet size no longer decreased significantly. A gas flow rate of 25 L min^{-1} was chosen as the condition for all subsequent reactions. The gas-spray microdroplet diameter was 35 μm under this condition.

It is critical to investigate the difference of the light intensity distribution between the gas-spray microdroplets reactor and the conventional bulk solution system. According to the results of numerical calculations, the photon transport attenuation effect was significant, and light intensity rapidly decreased because of the relatively high absorbance of photosensitizer in bulk solution. This phenomenon can be observed under a variety of different illumination methods, containing near-uniform illumination utilizing LED beads, sidewise illumination using a Xe lamp, and distributed illumination employing LED strips (Fig. 2b). Only the section closest to the reactor wall can effectively perform the photocatalytic reaction in bulk solution system, decreasing the illumination utilization efficiency. For a microdroplet reactor, the superimposed light resulted in a significantly improved light intensity because of the short light pathlength through photosensitizer-containing microdroplets. The overall light intensity in the gas-spray

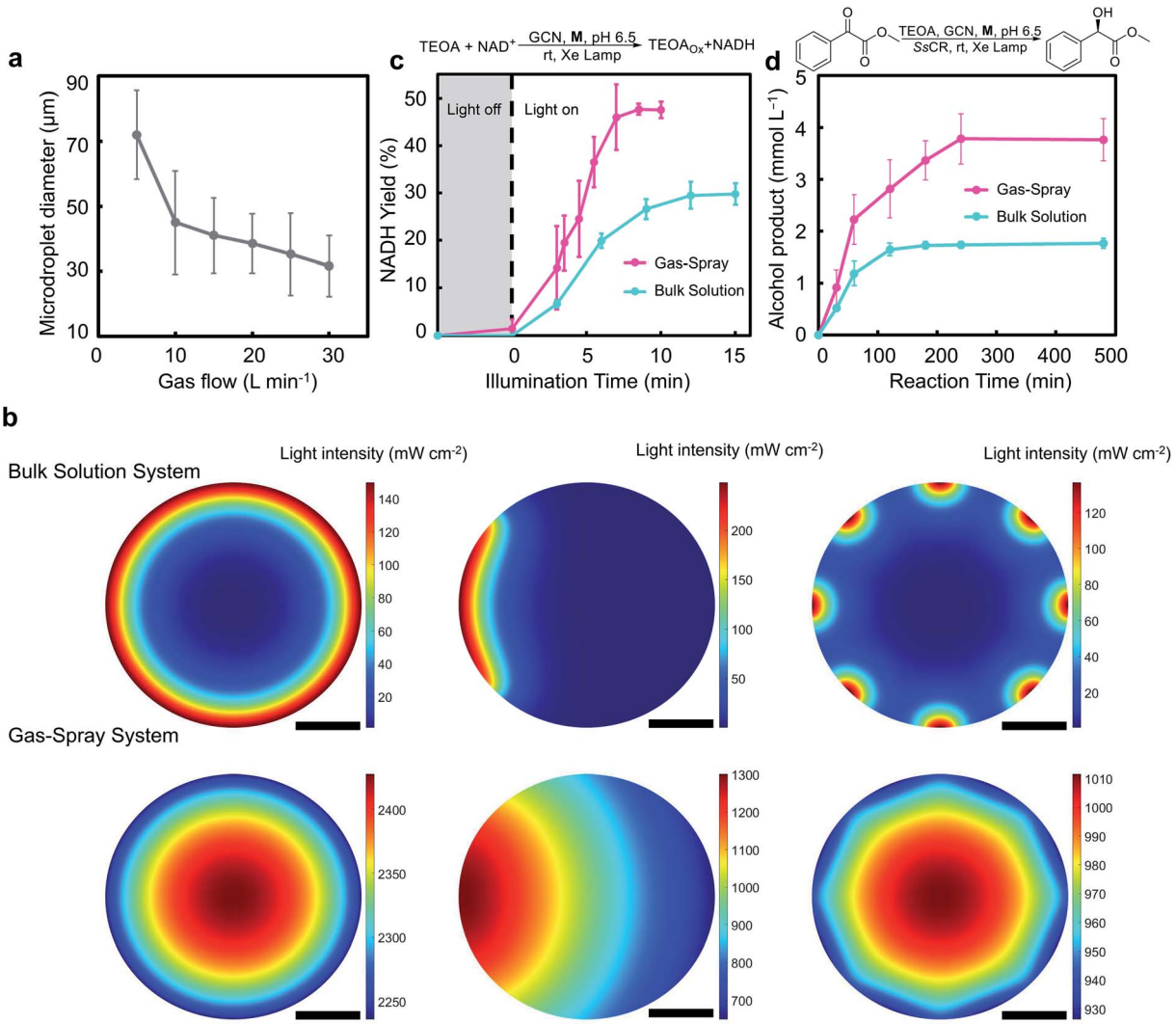

Fig. 2 Enhanced catalytic performance in gas-spray enzyme-photo-coupled (EPC) system. (a) Microdroplet diameter measured using a high-speed camera at different gas velocities. (b) Calculated light intensity distribution with different illumination methods in the gas-spray reactor and bulk solution system (shown as a heat map), first column, near-uniform illumination using LED beads, second column, sided illumination using Xe-lamp, third column, illumination using LED strip, scale bar, 5 cm. (c) Regeneration of reduced nicotinamide adenine dinucleotide in the gas-spray microdroplet reactor and bulk solution system. NAD^+, 1 mM; **M**, 0.2 mM; triethanolamine (TEOA), 400 mM; PBS buffer, 0.1 M (pH 6.5); graphite carbon-nitride (GCN), 0.33 mg mL^{-1}. (d) Enhanced reaction rate brought by the gas-spray EPC catalysis system. NAD^+, 1 mM; **M**, 0.2 mM; TEOA, 400 mM; PBS buffer, 0.1 M (pH 6.5); GCN, 0.33 g L^{-1}; *Sporobolomyces salmonicolor* carbonyl reductase (*Ss*CR), 1 g L^{-1}; substrate (methyl phenylglyoxylate, predissolved in 2% v/v dimethyl sulfoxide), 20 mM.

microdroplet reactor was significantly increased by 43.6–71.5 times compared to the bulk solution system. Meanwhile, considering that the microdroplets do not actually occupy the entire volume in the reactor, as well as that a light intensity lower than 125 mW cm^{-2} could not effectively drive the photocatalyzed NAD^+ regeneration process (Fig. S11†), correction terms were introduced to amend the actual energy utilization. The light energy utilization enhancement rate could still reach 1.2 to 1.4 times for a near-uniform and sidewise illumination system after the correction, in view of the fact that the microdroplets occupied only 0.95% of the reactor volume (details can be found in ESI Section 12†). The actual light energy utilization would also be enhanced with lower incident light intensity, reducing process operating costs. For instance, when LED strips were used for distributed illumination, due to its relatively low light intensity, the corrected light energy utilization enhancement rate could reach 22.5 times over traditional bulk solution system.

For systems with relatively low absorbance, constructing photocatalytic system in gas-sprayed microdroplets is also a promising method to enhance the reaction rate. In addition to the droplet could act as spherical lens to focus light and enhance the reaction rate,[41,42] microdroplets that meet certain refractive index requirements can form an optical confining domain, which could increase the light intensity and significantly enhance the photochemical reaction rate within the droplet.[53]

Photocatalytic cofactor regeneration in gas-spray microdroplets was performed under the abovementioned reaction

conditions. It was shown that the cofactor yield and reaction rate of the gas-spray microdroplet system were higher than those of the bulk solution system (Fig. 2c). In the gas-spray microdroplet photocatalytic cofactor regeneration system, 1.5% cofactor regeneration yield was detected after only one round of light illumination of reaction solution (which is equivalent to 5 s illumination). In comparison, no product was detected in the bulk solution system after 5 s illumination. While the bulk solution system only presented a 28% ± 2% regeneration of NADH after 10 min, 48% ± 2% regeneration of NADH was observed in a gas-spray microdroplet reactor within 10 min.

On the basis of the faster NADH regeneration in gas-spray reactor, the efficiency of EPC catalyzed chiral ketone reduction process was also enhanced. The reaction rate in the gas-spray reactor (TOF 3.5 ± 0.4 × 10^4 h^{-1}) was significantly higher than conventional bulk solution system (TOF 1.6 ± 0.1 × 10^4 h^{-1}), resulting in a 2.2-fold increase in the reaction rate (Fig. 2d, TOF was defined as the number of substrate molecules methyl phenylglyoxylate catalyzed by each *Ss*CR molecule after the first hour in EPC catalyzed chiral ketone reduction). In addition, the final product concentration detected in the gas-spray microdroplet reactor also showed a significant increase. Thus, more study into the mechanism of performance enhancement in microdroplets is required for a better understanding of the EPC catalysis in water microdroplets.

First, the distribution of reagents inside the microdroplet might be different from the uniform distribution in the bulk solution because of the higher specific surface area and larger surface energy of the microdroplet.[39] It is difficult to observe and analyze gas-spray microdroplets *in situ* because of the rapid droplet velocity, so we prepared microdroplets using ultrasonication to approximate the gas-spray microdroplets.[40] *Ss*CR was stained with rhodamine isothiocyanate (RITC), and microdroplets were observed using a confocal laser scanning microscope. It is observed that the enzyme was almost exclusively distributed at the border of the microdroplet, while almost no enzyme was detected inside the microdroplets (Fig. 3a). In contrast to the enzyme, GCN was uniformly distributed within the microdroplet (Fig. 3b, c and S12 in ESI†). This could be attributed to the microdroplet system's tendency to spontaneously reduce the surface energy of the system. Microdroplet surface area is several orders of magnitude greater than that of bulk solution system, which is a high surface Gibbs free energy system. The substrate, which is hydrophobic and has lower surface tension compared to water, tends to concentrate itself at the periphery of the microdroplet thus reducing the surface Gibbs free energy. Enzymes are amphiphilic,

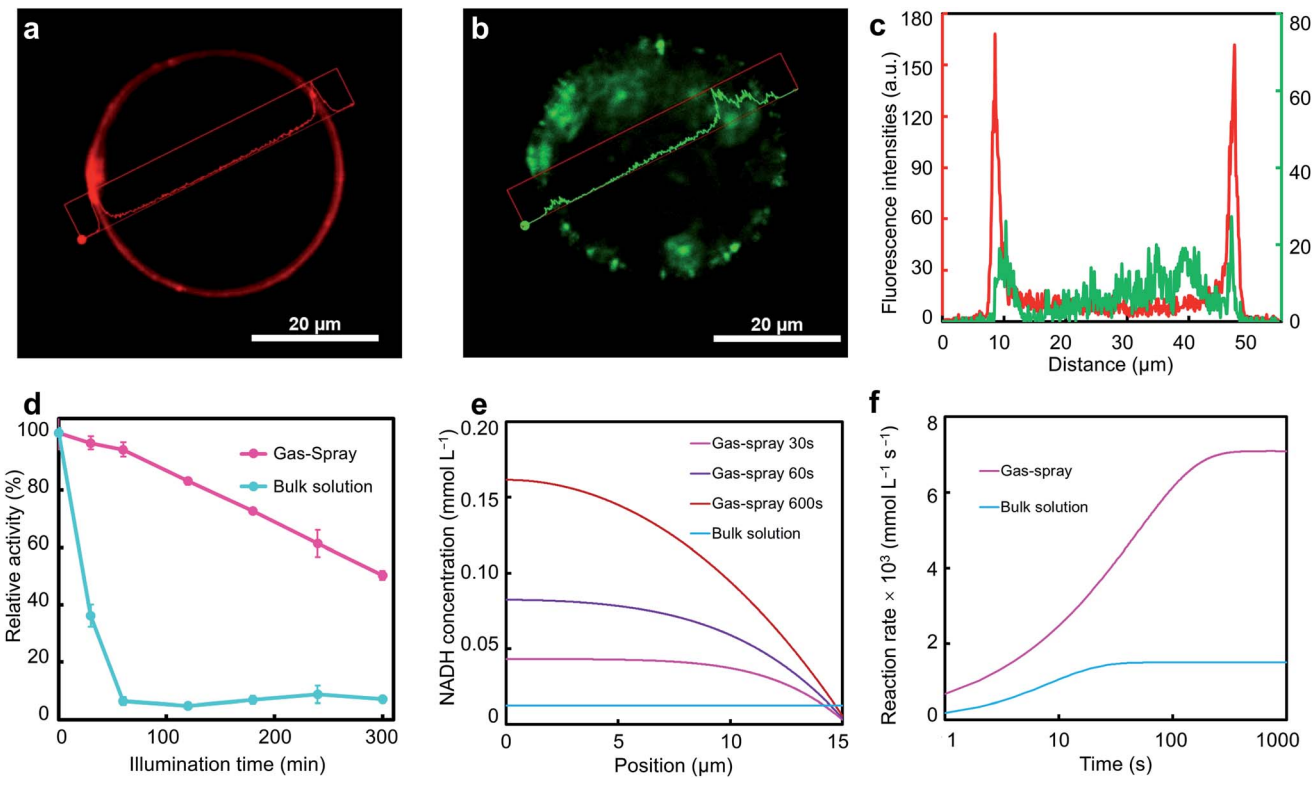

Fig. 3 Mechanism analysis of activity enhancement in microdroplets. (a and b) Distribution of enzyme and graphite carbon-nitride (GCN) in microdroplets, respectively, which is observed by staining enzymes with rhodamine isothiocyanate and laser confocal scanning microscopy. (a) Fluorescence image of the enzyme in microdroplets. (b) Fluorescence image of GCN in microdroplets. (c) Schematic of fluorescence intensity of the enzyme (red) and GCN (green). (d) Residual enzyme activity with time under light illumination in bulk solution and gas-spray reactor. (e) Calculated concentration distributions after different reaction times in microdroplets compared with the bulk solution system. (f) Calculated microdroplet-induced reaction rate enhancement.

leading to their distribution at the air–water interface, *i.e.*, the outer edge of microdroplets.[54] Although GCN is an organic semiconductor-type hydrophobic photosensitizer, because of its large hydrodynamic diameter (~2 μm, Fig. S6 in ESI†), it cannot be distributed on the microdroplet surface, but is only relatively uniformly distributed within microdroplets. Therefore, spontaneous control of enzyme and photosensitizer compartmentalization at the microscale was achieved.

Based on the above spontaneous microscale compartmentalized control, we hypothesize that this compartmentalized microdroplet can separate enzymes from GCN during catalytic processes, thus avoiding the inactivation of enzymes caused by direct contact with photogenerated holes arising from GCN.[25,27–29] Residual enzyme activities in gas-spray EPC catalysis and bulk solution systems were tested to determine the influence of light exposure on enzymes (details can be found in ESI Section 14†). The results showed that enzymes in bulk solution lost activity rapidly, leaving <10% activity within 60 min, which is also consistent with the catalytic test in which the maximum yield is achieved at ~60 min and no longer rises (Fig. 2d and 3d). In comparison, the enzyme in the gas-spray microdroplet maintained more than 50% of its activity after 5 h of illumination, similar to the remaining enzyme activity of the system without light (Fig. S13 in ESI†). This indicates that the microscale compartmentalization can effectively protect the enzyme activity.

In addition to prolonged residual enzyme activity, the highly regionalized distribution of different substances inside the microdroplet is very similar to the crowded but ordered environment *in vivo*.[55] It might be possible that the local reaction rate can be effectively increased to further improve the overall catalytic efficiency. Therefore, we performed theoretical calculations based on the distribution of the components within the microdroplet and bulk solutions (Fig. 3e, f, S14 and S15 in ESI†).

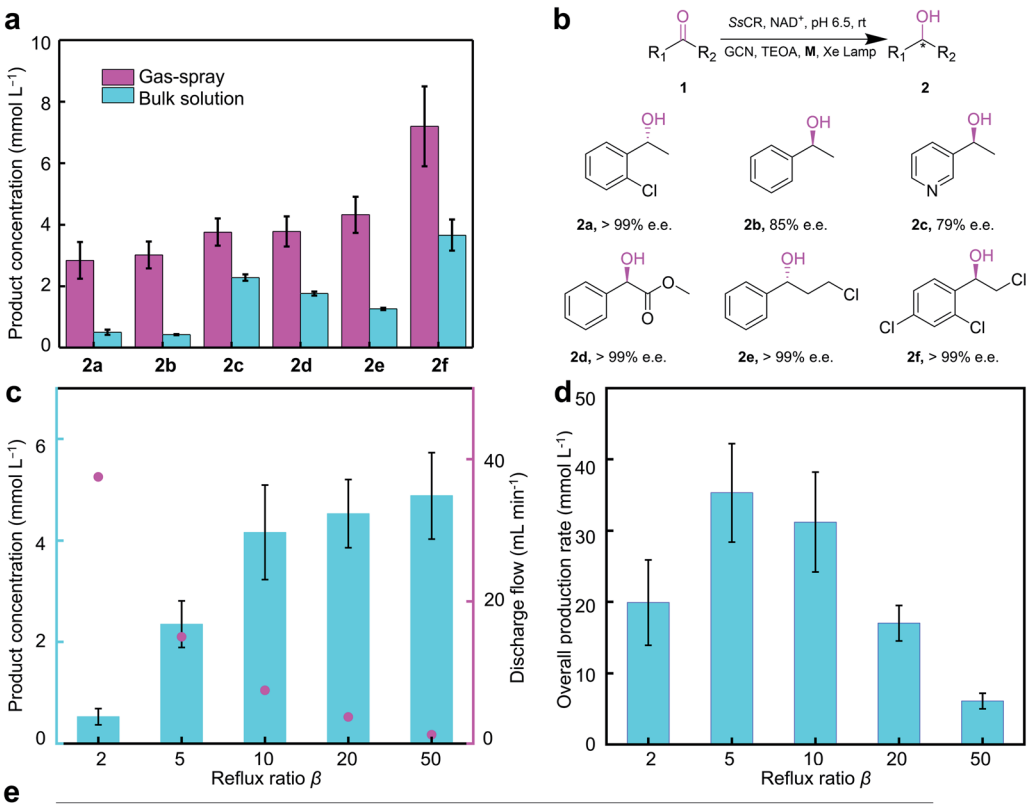

e

Chiral intermediate	2a	2d	2e	2f
Product concentration /mmol L^{-1}	2.9±1.0	4.2±0.9	4.5±0.6	7.7±1.5
e.e. /%	>99	>99	>99	>99
Overall production rate/μmol min^{-1}	22.0±7.2	31.2±7.0	33.4±4.7	57.6±11.4

Fig. 4 Comparison of EPC-catalyzed chiral alcohol synthesis in bulk solution system and gas-spray system, and the continuous chiral alcohol synthesis using gas-spray system. (a) Final concentration of products **2a–2f**. (b) Selectivity of products **2a–2f**. GCN, graphite carbon-nitride; NAD, nicotinamide adenine dinucleotide; SsCR, *Sporobolomyces salmonicolor* carbonyl reductase; TEOA, triethanolamine. Note that according to the sequence rule of chiral compounds, there are differences in the stereo configuration of **2a–2f**, which is in consistent with previous report.[51,52] (c) Variation of product concentration and outlet flow rate with reflux ratio β. Product concentration (blue column) is plotted on the left axis and the outlet flow rate (pink dot) is plotted on the right axis. (d) Overall production rate under different β conditions. (e) Effects of chiral pharmaceutical intermediates continuous synthesis process.

A different concentration distribution with faster reaction rates was observed in microdroplets. The concentration of NADH in microdroplets gradually increased as the reaction proceeded, whereas the bulk solution system concentration remained constant after equilibrium was reached. This concentration distribution is markedly different from the relatively homogeneous distribution produced by sufficient stirring in bulk solution. Notably, the calculations showed that in the microdroplet system, the NADH concentration near the microdroplet surface was slightly lower compared to the solution system due to the diffusion limitation of cofactors and electron mediators, which would reduce the overall reaction rate somehow. However, the proximity effect from the regional distribution still brought about a significant enzyme-catalyzed reaction rate enhancement (~4.7 times). The localized high reaction rate brought about by the regionalization effect would further reduce the NADH concentration near the surface, leading to a higher cofactor concentration gradient and thus enhancing the diffusion efficiency within the microdroplet. This phenomenon demonstrated that the proximity effect generated from regionalized distribution in such microdroplets holds the possibility of higher reaction rates. This feature, combined with higher residual enzyme activity, enabled the significant reaction rate enhancement within microdroplets.

The EPC catalysis in gas-spray microdroplets was subsequently applied to the asymmetric synthesis of several chiral alcohols (Fig. 4 and S16–S33 in ESI.† **2a**, (*R*)-1-(2-chlorophenyl) ethanol; **2b**, (*S*)-1-phenylethanol; **2c**, (*S*)-1-(3-pyridyl)ethanol; **2d**, (*R*)-methyl mandelate; **2e**, (*R*)-3-chloro-1-phenyl-1-propanol; **2f**, (*R*)-2-chloro-1-(2,4-dichlorophenyl)ethanol). It gave much higher final product concentrations for the synthesis of different chiral alcohols, such as the intermediates of clorprenaline (β2-adrenergic agonist, **2a**), dapoxetine (selective serotonin reuptake inhibitor, **2e**) and miconazole (antifungal, **2f**) compared with conventional catalysis in bulk solution. Final product concentration was increased up to 5.6-fold. This result showed that the gas-spray EPC catalysis system is a promising platform to achieve large-scale synthesis of pharmaceutical intermediates. Meanwhile, it is noted that among the products tested (Fig. 4a), the yield of **2c** in the gas-spray system was similar to the bulk solution system. This behavior might be from the fact that **1c** is readily soluble in water compared to other substrates, resulting in a substrate distribution that is inconsistent with the properties of compartmentalization in microdroplets.

Moreover, with the continuous operating characteristics of gas-sprayed microdroplet reactor, continuous enzyme-photo-coupled synthesis of chiral intermediates was implemented (Fig. 4). The continuous synthesis process could be optimized by adjusting the reflux ratio β, which is defined as the ratio of reflux flow and discharge flow. As shown in Fig. 4a and b, with the increase of β, product concentration increased significantly, while overall production rate showed a volcano curve. Considering the subsequent purification, β setting of 10 was more appropriate. Based on the optimized continuous reaction condition, chiral pharmaceutical intermediates **2a**, and **2a–2f** were successfully achieved (Fig. 4c), indicating that gas-sprayed microdroplet reactor could be a practical and universal platform for enzyme-photo-coupled synthesis of chiral intermediates.

Experimental

Materials

Oxidized nicotinamide adenine dinucleotide (NAD^+), TEOA, RITC, and 2,2′-bipyridine were purchased from Sigma-Aldrich (St. Louis, MO, USA). Dichloro(pentamethylcyclopentadienyl) rhodium(III) dimer and *n*-nonane were purchased from Meryer (Shanghai, China). Urea, ethyl acetate, and reagents for preparing buffers were purchased from Sinopharm (China). Other chemicals are all of the analytical grades and were used as received without further purification.

Synthesis of graphite carbon-nitride

GCN was synthesized based on a procedure described in a previous paper.[56] In detail, 50 grams of urea were heated in static air at 550 °C for 4 h with a ramp rate of 5 °C min^{-1}. The resulting yellow agglomerates were dispersed in water and ultrasound etched for 12 h, followed by vacuum drying. The collected yellow powder was then thermally oxidized etched in static air at 500 °C for 2 h with a ramp rate of 3 °C min^{-1}. A light-yellow powder (GCN) was finally obtained with an overall yield of ~0.6%. The approximate composition of GCN is determined to be $C_3N_{4.47}H_x$ using elemental analysis.

Photocatalytic regeneration of reduced nicotinamide adenine dinucleotide in bulk solution

The photocatalytic regeneration of NADH in bulk solution was conducted in a quartz cuvette (3 mL). First, 100 mM PBS buffer (pH 6.5) containing 0.33 g L^{-1} GCN, 1 mM NAD^+, 0.2 mM **M**, and 400 mM TEOA was placed in the quartz cuvette. After incubation in darkness for 30 min, the quartz cuvette was illuminated using a xenon lamp source (Beijing Perfectlight, PLS-SXE300D, 450 W) with a 400 nm cutoff filter. The distance between the cuvette and light source was 25 cm to avoid a significant increase in the system temperature, and the light intensity on the quartz cuvette was measured to be 1000 mW cm^{-2} using a radiation meter. The concentration of NADH was determined by measuring the absorbance at 340 nm using an ultraviolet-visible (UV-vis) spectrophotometer (SHIMADZU, UV-2600) at room temperature. The molar absorption coefficient for NADH was 6220 M^{-1} cm^{-1}.

Photocatalytic regeneration of reduced nicotinamide adenine dinucleotide in gas-spray microdroplet reactor

The photocatalytic regeneration of NADH in microdroplets was conducted in gas-spray microdroplet reactor. First, 100 mL 100 mM PBS buffer (pH 6.5) of the reaction solution containing 0.33 g L^{-1} GCN, 1 mM NAD^+, 0.2 mM **M**, and 400 mM TEOA was placed in a storage tank. Furthermore, the gas-spray process was activated in the absence of illumination for 30 min. During the gas-spray process, the nitrogen flow was set to 25 L min^{-1} and solution flow was set to 100 mL min^{-1}. After gas-spray in

darkness for 30 min, the reactor was illuminated using the xenon lamp source (Beijing Perfectlight, PLS-SXE300D, 450 W) with a 400 nm cutoff filter. The concentration of NADH was determined by measuring the absorbance at 340 nm using a UV-vis spectrophotometer (SHIMADZU, UV-2600). The molar absorption coefficient for NADH was 6220 M^{-1} cm^{-1}.

Enzyme-photo-coupled catalyzed reduction of chiral alcohols

EPC catalyzed reduction of chiral alcohol was conducted under room temperature, illuminated using a xenon lamp source with a 400 nm cutoff filter (Beijing Perfectlight, PLS-SXE300D, 450 W). The reaction solution was 100 mM PBS buffer (pH 6.5) containing 0.33 g L^{-1} GCN, 1 mM NAD^+, 0.2 mM **M**, 1 g L^{-1} *Ss*CR, 400 mM TEOA, and 20 mM substrate (predissolved in 2% v/v dimethyl sulfoxide). For the reaction in the bulk solution, a 3 mL reaction solution was added to the quartz cuvette. The distance between the cuvette and light source was 25 cm, and the light intensity on the quartz cuvette was measured to be 1000 mW cm^{-2} using a radiation meter. For the reaction in the gas-spray microdroplet reactor, a 100 mL reaction solution was placed in the storage tank. The nitrogen flow was set to 25 L min^{-1} and solution flow was set to 100 mL min^{-1}. The samples were collected, followed by extraction with twice the volume of ethyl acetate, then dried with anhydrous magnesium sulfate and analyzed using UV-vis absorbance on high-performance liquid chromatography (HPLC; Dalian Elite, Agress 1100) equipped with a chiral column (CHIRALCEL® OB-H, 250 × 4.6 mm, 10 μm Φ); flow rate: 0.25 mL min^{-1}; λ: 210 nm; mobile phase: 2.5% (v/v) isopropanol in hexanes; temperature: 40 °C. The HPLC conditions can have subtle differences for different substances and products. Specific HPLC conditions can be found in the ESI Section 15, Table S1.†

Imaging of microdroplets

To prepare microdroplets, 1 mL reaction solution containing 100 mM PBS buffer (pH 6.5), 0.33 g L^{-1} GCN, and 1 g L^{-1} RITC-labeled *Ss*CR were mixed with 10 mL *n*-nonane in a microtube, placed in a bath sonicator (Kunshan KQ-300DE), and was sonicated for 2 min at room temperature. The prepared microdroplets were cast onto a glass slide and imaged using a confocal microscope (LSM 710 Meta, Carl Zeiss, GmbH, Germany). The fluorescence signals were recorded with excitation laser beams (405 nm for GCN and 488 nm for RITC-labeled *Ss*CR) and their preprogrammed emission windows. The total frame time for a 512 × 512 pixel image was 0.8 s. The acquired images and fluorescence intensities were processed with the ZEN software suite (Carl Zeiss GmbH, Germany).

Conclusions

In summary, a gas-spray EPC catalysis system was constructed. An improved solar energy utilization (43.6–71.5 times) and higher final product concentrations (1.5–5.6 folds) of chiral alcohols were experimentally and theoretically demonstrated, compared with conventional catalysis in bulk solution. The mechanism of the highly improved catalysis in the gas-spray microdroplet was investigated. Higher solar energy utilization and light intensity of microdroplets, and a highly regionalized distribution of substances, are proved to be the origin of better catalytic performance. Furthermore, the gas-spray reactor is suitable for scaling-up and continuous operation.

Data availability

The data that support the findings of this study are available in the main manuscript, the ESI† and also from the authors upon reasonable request.

Author contributions

J. G. conceived the idea. Yunxiu B. and P. L. performed the experiments. Yunpeng B. provided *Ss*CR. Yunxiu B. performed the numerical calculations. Yunxiu B., P. L., R. N. Z. and J. G. wrote the paper.

Conflicts of interest

The authors declare no competing interests.

Acknowledgements

This work was supported by the National Key Research and Development Program of China (2021YFC2102800). R. N. Z. thanks the US Air Force Office of Scientific Research through the Multidisciplinary University Research Initiative (MURI) program (AFOSR FA9550-21-1-0170).

Notes and references

1 N. J. Planavsky, D. Asael, A. Hofmann, C. T. Reinhard, S. V. Lalonde, A. Knudsen, X. Wang, F. O. Ossa, E. Pecoits, A. J. B. Smith, N. J. Beukes, A. Bekker, T. M. Johnson, K. O. Konhauser, T. W. Lyons and O. J. Rouxel, *Nat. Geosci.*, 2014, **7**, 283–286.
2 A. Fujishima and K. Honda, *Nature*, 1972, **238**, 37–38.
3 E. Reisner, D. J. Powell, C. Cavazza, J. C. Fontecilla-Camps and F. A. Armstrong, *J. Am. Chem. Soc.*, 2009, **131**, 18457–18466.
4 K. A. Brown, M. B. Wilker, M. Boehm, G. Dukovic and P. W. King, *J. Am. Chem. Soc.*, 2012, **134**, 5627–5636.
5 K. Bourzac, *Proc. Natl. Acad. Sci. U. S. A.*, 2016, **113**, 4545–4548.
6 N. Dong Heon, J. Z. Zhang, V. Andrei, N. Kornienko, N. Heidary, A. Wagner, K. Nakanishi, K. P. Sokol, B. Slater, I. Zebger, S. Hofmann, J. C. Fontecilla-Camps, C. B. Park and E. Reisner, *Angew. Chem., Int. Ed.*, 2018, **57**, 10595–10599.
7 R. K. Yadav, J.-O. Baeg, G. H. Oh, N.-J. Park, K.-j. Kong, J. Kim, D. W. Hwang and S. K. Biswas, *J. Am. Chem. Soc.*, 2012, **134**, 11455–11461.
8 X. Ji, Z. Su, P. Wang, G. Ma and S. Zhang, *Small*, 2016, **12**, 4753–4762.

9 S. K. Kuk, R. K. Singh, D. H. Nam, R. Singh, J.-K. Lee and C. B. Park, *Angew. Chem., Int. Ed.*, 2017, **56**, 3827–3832.
10 J. H. Kim, D. H. Nam and C. B. Park, *Curr. Opin. Biotechnol.*, 2014, **28**, 1–9.
11 K. A. Brown, M. B. Wilker, M. Boehm, H. Hamby, G. Dukovic and P. W. King, *ACS Catal.*, 2016, **6**, 2201–2204.
12 X. Lang, J. Zhao and X. Chen, *Chem. Soc. Rev.*, 2016, **45**, 3026–3038.
13 W. Zhang, E. Fernandez-Fueyo, Y. Ni, M. van Schie, J. Gacs, R. Renirie, R. Wever, F. G. Mutti, D. Rother, M. Alcalde and F. Hollmann, *Nat. Catal.*, 2018, **1**, 55–62.
14 Y. Wu, J. Shi, D. Li, S. Zhang, B. Gu, Q. Qiu, Y. Sun, Y. Zhang, Z. Cai and Z. Jiang, *ACS Catal.*, 2020, **10**, 2894–2905.
15 M. A. Emmanuel, N. R. Greenberg, D. G. Oblinsky and T. K. Hyster, *Nature*, 2016, **540**, 414–417.
16 K. F. Biegasiewicz, S. J. Cooper, X. Gao, D. G. Oblinsky, J. B. Kim, S. E. Garfinkle, L. A. Joyce, B. A. Sandoval, G. D. Scholes and T. K. Hyster, *Science*, 2019, **364**, 1166–1169.
17 X. Ding, C.-L. Dong, Z. Guan and Y.-H. He, *Angew. Chem., Int. Ed.*, 2019, **58**, 118–124.
18 J. S. DeHovitz, Y. Y. Loh, J. A. Kautzky, K. Nagao, A. J. Meichan, M. Yamauchi, D. W. C. MacMillan and T. K. Hyster, *Science*, 2020, **369**, 1113–1118.
19 X. Huang, B. Wang, Y. Wang, G. Jiang, J. Feng and H. Zhao, *Nature*, 2020, **584**, 69–74.
20 K. A. Brown, D. F. Harris, M. B. Wilker, A. Rasmussen, N. Khadka, H. Hamby, S. Keable, G. Dukovic, J. W. Peters, L. C. Seefeldt and P. W. King, *Science*, 2016, **352**, 448–450.
21 E. Edwardes Moore, V. Andrei, S. Zacarias, I. A. C. Pereira and E. Reisner, *ACS Energy Lett.*, 2020, **5**, 232–237.
22 X. Ji, Y. Kang, T. Fan, Q. Xiong, S. Zhang, W. Tao and H. Zhang, *J. Mater. Chem. A*, 2020, **8**, 323–333.
23 K. Chen and F. H. Arnold, *Nat. Catal.*, 2020, **3**, 203–213.
24 Y. S. Nam, A. P. Magyar, D. Lee, J.-W. Kim, D. S. Yun, H. Park, T. S. Pollom Jr, D. A. Weitz and A. M. Belcher, *Nat. Nanotechnol.*, 2010, **5**, 340–344.
25 S. Zhang, J. Shi, Y. Sun, Y. Wu, Y. Zhang, Z. Cai, Y. Chen, C. You, P. Han and Z. Jiang, *ACS Catal.*, 2019, **9**, 3913–3925.
26 Y. Su, K. Kuijpers, V. Hessel and T. Noel, *React. Chem. Eng.*, 2016, **1**, 73–81.
27 Y. Bai, L. Wang and J. Ge, *Syst. Microbiol. Biomanuf.*, 2021, **1**, 245–256.
28 S. Zhang, S. Liu, Y. Sun, S. Li, J. Shi and Z. Jiang, *Chem. Soc. Rev.*, 2021, **50**, 13449–13466.
29 N. Yang, Y. Tian, M. Zhang, X. Peng, F. Li, J. Li, Y. Li, B. Fan, F. Wang and H. Song, *Biotechnol. Adv.*, 2022, **54**, 107808.
30 M. Girod, E. Moyano, D. I. Campbell and R. G. Cooks, *Chem. Sci.*, 2011, **2**, 501.
31 S. Banerjee and R. N. Zare, *Angew. Chem., Int. Ed.*, 2015, **54**, 14795–14799.
32 D. N. Mortensen and E. R. Williams, *J. Am. Chem. Soc.*, 2016, **138**, 3453–3460.
33 X. Yan, R. M. Bain and R. G. Cooks, *Angew. Chem., Int. Ed.*, 2016, **55**, 12960–12972.
34 J. K. Lee, K. L. Walker, H. S. Han, J. Kang, F. B. Prinz, R. M. Waymouth, H. G. Nam and R. N. Zare, *Proc. Natl. Acad. Sci. U. S. A.*, 2019, **116**, 19294–19298.
35 Z. Wei, Y. Li, R. G. Cooks and X. Yan, in *Annual Review of Physical Chemistry*, ed. M. A. Johnson and T. J. Martinez, 2020, vol. 71, pp. 31–51.
36 X. Zhong, H. Chen and R. N. Zare, *Nat. Commun.*, 2020, **11**, 1049.
37 P. Zhao, H. P. Gunawardena, X. Zhong, R. N. Zare and H. Chen, *Anal. Chem.*, 2021, **93**, 3997–4005.
38 X. Zhong, H. Chen and R. N. Zare, *QRB Discovery*, 2021, **2**, e4.
39 J. K. Lee, D. Samanta, H. G. Nam and R. N. Zare, *J. Am. Chem. Soc.*, 2019, **141**, 10585–10589.
40 S. Lhee, J. K. Lee, J. Kang, S. Kato, S. Kim, R. N. Zare and H. G. Nam, *Sci. Adv.*, 2020, **6**, eaba0181.
41 C. Favre, V. Boutou, S. C. Hill, W. Zimmer, M. Krenz, H. Lambrecht, J. Yu, R. K. Chang, L. Woeste and J. P. Wolf, *Phys. Rev. Lett.*, 2002, **89**, 35002.
42 S. Nagelberg, L. D. Zarzar, N. Nicolas, K. Subramanian, J. A. Kalow, V. Sresht, D. Blankschtein, G. Barbastathis, M. Kreysing, T. M. Swager and M. Kolle, *Nat. Commun.*, 2017, **8**, 14673.
43 B. J. Finlayson-Pitts, *Chemistry of the upper and lower atmosphere: theory, experiments, and applications*, Academic Press, San Diego, California, 2000.
44 K. Y. Kim and W. R. Marshall, *AIChE J.*, 1971, **17**, 575–584.
45 P. D. Hede, P. Bach and A. D. Jensen, *Chem. Eng. Sci.*, 2008, **63**, 3821–3842.
46 J. Liu and M. Antonietti, *Energy Environ. Sci.*, 2013, **6**, 1486–1493.
47 Z. Tong, D. Yang, Z. Li, Y. Nan, F. Ding, Y. Shen and Z. Jiang, *ACS Nano*, 2017, **11**, 1103–1112.
48 D. Yang, Y. Zhang, S. Zhang, Y. Cheng, Y. Wu, Z. Cai, X. Wang, J. Shi and Z. Jiang, *ACS Catal.*, 2019, **9**, 11492–11501.
49 H. C. Lo, C. Leiva, O. Buriez, J. B. Kerr, M. M. Olmstead and R. H. Fish, *Inorg. Chem.*, 2001, **40**, 6705–6716.
50 F. Hollmann, B. Witholt and A. Schmid, *J. Mol. Catal. B: Enzym.*, 2002, 167–176.
51 M. Kataoka, K. Kita, M. Wada, Y. Yasohara, J. Hasegawa and S. Shimizu, *Appl. Microbiol. Biotechnol.*, 2003, **62**, 437–445.
52 Y.-Q. Zhang, T.-T. Feng, Y.-F. Cao, X.-Y. Zhang, T. Wang, M. R. H. Nina, L.-C. Wang, H.-L. Yu, J.-H. Xu, J. Ge and Y.-P. Bai, *ACS Catal.*, 2021, **11**, 10487–10493.
53 P. C. Arroyo, G. David, P. A. Alpert, E. A. Parmentier, M. Ammann and R. Signorell, *Science*, 2022, **376**, 293–296.
54 P. W. Atkins, *Atkins' physical chemistry*, Oxford Univ. Press, Oxford, 10th edn, 2014.
55 P. Jordan, P. Fromme, H. T. Witt, O. Klukas, W. Saenger and N. Krauss, *Nature*, 2001, **411**, 909–917.
56 P. Niu, L. Zhang, G. Liu and H.-M. Cheng, *Adv. Funct. Mater.*, 2012, **22**, 4763–4770.